4-30-2021

A Differential Equations Model of Circulatory System Hemodynamics

Allison Newman
University of Richmond

A Differential Equations Model of Circulatory System Hemodynamics

by

Allison Newman

Honors Thesis

Submitted to:

Mathematics Department
University of Richmond
Richmond, VA

April 30, 2021

Advisor: Dr. Lester Caudill

Chapter 1

Introduction

1.1 Background

Our internal organs (or, more precisely, organ systems) do not operate in isolation from one another. Consequently, dysfunction in one organ system often affects others, sometimes exacerbating the original dysfunction. For instance, pneumonia (an infection of the respiratory system) can result in insufficient oxygen to the kidneys, reducing their ability to filter wastes from the blood, and resulting in abnormally high levels of waste in the blood [9, 17, 41, 28]. This, in turn, can affect both cardiac and respiratory function, leading to an even lower oxygen supply for the kidneys, so kidney function is further compromised, and the patient rapidly declines from an unseen negative feedback loop operating inside them [10, 25]. In the medical community, this is known as *sequential organ failure (SOF)*, and this can arise from trauma, serious infection (leading to sepsis), or in a "regular" illness, when comorbidities (i.e. pre-existing health conditions) are present [31]. In intensive care units (ICUs), healthcare professionals routinely use scoring systems like the *Sequential Organ Failure Assessment (SOFA)* to predict the likelihood of death in a patient with SOF [22].

It is not an exaggeration to describe the human circulatory (i.e. cardiovascular) system as

the body's main transport system. This system, consisting of the heart and all blood vessels, is the main physical interconnection between the main organ systems, as it carries nutrients and wastes from one organ to another, linking these systems into a single complex network. Dr. Lester Caudill's research lab is actively engaged in developing a mathematical model of this organ system network, with the long-term goal of investigating treatment options (via model simulations) for medical conditions (especially pneumonia and sepsis [11]) that lead to SOF.

Logically, a model of this network should begin with the circulatory system as its foundation. At its core, an acceptable (for our purposes) mathematical model of the circulatory system must meet certain design criteria:

- reflect the key functionality of the system (e.g. beating heart, pressure-driven blood circulation).
- include the ability of our system model to transport nutrients and wastes through the system (including a second organ system) via blood flow dynamics.
- be mathematically simple enough to be expandable to include models of other organ systems.

This research focuses on developing a circulatory system differential equations model that meets these design criteria.

This thesis is organized as follows: Chapter 1 provides the physiological background of the circulatory system and its function, which will serve as a basis for our model. We develop and present our model in Chapter 2. In Chapter 3, we conduct some model validation via several numerical proof-of-concept demonstrations. Chapter 4 presents a strategy for modeling the transport of substances via our model's "blood," as well as a potential application to the evaluation of anti-hypertensive treatments. We conclude our work, and this thesis, in Chapter 5.

1.2 Previous Models

Over the years, various approaches to modeling the circulatory system have been published. The assumptions of these models and their respective goals vary greatly, influencing both their potential applications and their limitations. Although our model applies very similar physiological principles, we seek to simulate more macro-level effects.

Arthur C. Guyton is one of the most prominent and early figures to publish circulatory system modeling research. He determined that previous models had not incorporated all of the long-term regulation mechanisms, including the relationship between body fluid volumes and systemic function through a negative feedback loop [16]. For example, an increase in arterial pressure is balanced out by a decrease in body fluid volume and venous return. Guyton focused his studies on exploring the relationship between hypertension and the renal system [15], but he did not closely examine organ-organ dynamics. In the future, we hope to provide mathematical modeling insight on this.

In the Neal & Bassingthwaighte 2007 model, baroreceptor control was included to account for time-independent cardiac elastance [29]. The model was implemented to predict hemodynamic responses from acute hemorrhage while validating the outcomes with pig hemorrhage experiments. It most notably differs from our model by the inclusion of baroreceptor control, coronary circulation, nonlinear resistances for systemic circulation, and ventricular elastance. However, both of our models share the expression of pressure as a function of the difference of total blood volume and unstressed volume.

Albanese et al. 2016 model incorporates an in-depth simulation of pulmonary capillary blood and alveolar air exchange along with central nervous system regulation mechanisms [2]. While the flow rate functions resemble the functions that we use, they additionally incorporate tissue gas exchange flow rates for the major organ systems. They arrange these organs as parallel circuits; we plan to use a similar method once we are ready to add the

major organ systems.

Ursino & Magosso 2000 assume that the atria have passive compliance and the beating mechanism of the heart creates active ventricular compliance [46]. This decision prompted us to consider the atria as insignificant compared to the thick walls and muscular strength of the ventricles. For our model, the atria do not contract alongside the ventricles.

While previous models incorporate complex mechanisms of long-term regulation and establish many nonlinear relationships, we seek to present a more simplified system. Since the circulatory system will be a part of a network of inter-connected organs at a later time, a more simplistic model makes the overall organ systems model more manageable.

1.3 Key Cardiac Functionality

The circulatory system relies on a predictable cyclic repetition of beating ventricles to pump blood to the rest of the body. Cardiac cycle, which is one complete period of a heartbeat, is approximately 0.8 seconds long with a rate of 75 beats per minute (bpm) [20]. The normal cardiac output is around 4-7 L/min [27]. The heart contains four flow-control valves connected to the ventricles. They include the mitral and tricuspid valves, known together as the atrioventricular (AV) valves, and the aortic and pulmonary valves, known together as the semilunar (SL) valves (Figure 2.1). The mitral valve regulates flow from the left atrium to the left ventricle, the tricuspid valve regulates flow from the right atrium to the right ventricle, the aortic valve regulates flow from the left ventricle to the aorta, and the pulmonary valve regulates flow from the right ventricle to the pulmonary artery [20].

Along with the ventricles, the valves operate on their own schedule. The SL valves are open for roughly 0.21 seconds and the AV valves are open for 0.46 seconds during a single cardiac cycle [27]. The opening of the valves is driven by blood pressure gradients between the ventricle and the blood vessel that the valve is located between. There are also two

special cases for when both sets of valves are closed. During isovolumetric contraction, the ventricles contract and ventricular pressure rises for the SL valves to open. During isovolumetric relaxation, the ventricles relax and ventricular pressure decreases for the AV valves to open. In both scenarios, ventricular blood volume is unchanged from the closure of the valves.

The ventricles eject blood directly following isovolumetric contraction. This blood, termed stroke volume (SV), is defined as the volume of ejected blood that enters the target artery per beat. It is often associated with the rapid discharge of blood into the aorta. The mathematical formula is given by the difference between ventricular end-diastolic volume (VEDV) and end-systolic volume (VESV). A UK sudy found the following normal reference ranges for women: LVEDV = 124 mL, LVESV = 49 mL, RVEDV = 130 mL, and RVESV = 55 mL. For men, LVEDV = 166 mL, LVESV = 69 mL, RVEDV = 182 mL, and RVESV = 85 mL [34]. "L" stands for left and "R" stands for right.

The Frank-Starling Law is another important concept, particularly governing the idea that both ventricles output the same stroke volume. Since both sides of the heart contract almost simultaneously, cardiac output must be fairly equivalent on both sides of the heart to ensure that blood is not pooling up in the lungs [12]. The length of the cardiac muscle fibers is not the only determinant of ejection force though [7]. Stroke volume is directly related to preload and afterload. If central venous pressure increases (preload), then the pressure gradient will drive an increase in blood into the ventricle. The increase in volume of blood will stretch the muscular fibers of the myocardium and the heart will contract with greater force, releasing more blood into the aorta. Similarly, greater aortic pressure (afterload) decreases the pressure gradient and limits the blood flow out of the ventricle [48]. The next section further elaborates on the role of pressure gradients and other hemodynamic parameters in mediating blood flow between any two blood vessels.

1.4 Introduction to Hemodynamics

With numerous fluid dynamic principles available, scientists and mathematicians have creatively translated these laws for blood flow in the circulatory system. Jean Leonard Marie Poiseuille performed scientific experiments to identify the relationship, now known as Poiseuille's Law, between length L, viscosity μ, diameter D, the flow rate Q of fluids through the tube, and the pressure gradient ΔP. Equation (1.1) shows a common derivation of Poiseuille's Law [42].

$$Q = \frac{\pi D^4 \Delta P}{128 \mu L} \tag{1.1}$$

Poiseuille's Law exhibits how the direction and magnitude of blood flow is dependent on the pressure exerted in the current location and the pressure exerted in the intended location. In broad terms, flow rate Q is a function of resistance of a tube R and the difference ΔP between the pressures entering the tube and leaving the tube. This proportional relationship has been shown to hold in even the the thinnest compartments in the circulatory system, the capillaries. The Hagen-Poiseuille Law in Equation (1.2) captures flow between two blood vessels [7].

$$Q = \frac{\Delta P}{R} \tag{1.2}$$

Volume of blood and blood pressure are proportional to each other through a quantity known as compliance. Homer Warner [47] may have been the first cardiologist to explain that average ventricular compliance values change from systolic to diastolic phase. Compliance can be thought of as the general "stretchiness" of a blood vessel or ventricle and its ability to accommodate increasing volumes of blood. The general relationship between compliance, pressure, and volume is defined in Equation (1.3).

$$C = \frac{\Delta V}{\Delta P} \tag{1.3}$$

Blood vessels that have a high compliance are able to accommodate increasing blood volume without exerting much pressure. On average, venous compliance is 30 times greater than arterial compliance [18]. It is essential to maintain a high venous compliance since the veins carry a large percentage of the total blood volume, and increased venous stiffness can lead to adverse cardiovascular events such as hypertension [32]. Compliance eventually decreases as we age and the walls of the blood vessels become hardened.

The equations introduced in this section serve as the framework of our circulatory system model, and they will be referenced as we introduce our complementary equations.

Chapter 2

The Model

2.1 Compartment Diagram and Variables

Our circulatory system model includes the four-chambered heart, major blood vessels, lungs, and a generic organ as a placeholder for systemic organs. The model compartments and relevant blood flows are represented with a compartment diagram (Figure 2.1). In order to simplify the structure of the circulatory system, arterial and venous blood vessels are grouped into single compartments. These compartments only include the larger vessels with higher blood pressure, such as the aorta, large arteries, and proximal pulmonary arteries. The smaller arterioles and capillaries are included in the lung and generic organ compartments, where blood pulsation effects greatly diminish from the distribution of blood through these delicate and highly resistant tubes. This structure allows for the arteries compartment to reflect aortic blood pressure, the most common metric used by doctors.

The left atrium and right atrium, which contract slightly before their ventricular counterparts, are placed with the pulmonary veins and systemic veins. Since researchers appear to use central venous pressure or atrial pressure as the preload mechanism of stroke volume, it is presumed that the atria have similar parameters as the venous system [29], [7].

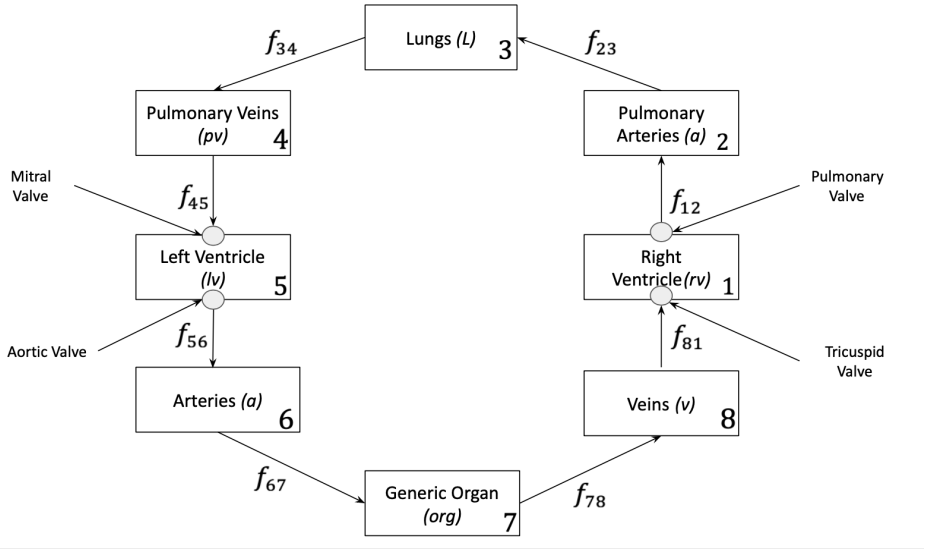

Figure 2.1: Compartment diagram for the proposed circulatory system model. For every adjacent pair of compartments i and j, there is a fate function f_{ij} that governs the blood flow from i to j.

In our model, time is the independent variable and the 8 dependent variables depict the blood volume in each of the 8 compartments. Additionally, we include blood pressure as an intermediate variable to reflect the relationship between volume and pressure (Table 2.1). Change in blood volume $\frac{dB_i}{dt}$ for a compartment i is the difference of the flow rate in and the flow rate out (Equations (2.1) - (2.8)). With the differential equations now constructed as a difference in flow rates, our next task is to specify the mathematical forms for the rate functions f_{ij}.

$$\frac{dB_{rv}}{dt} = f_{81} - f_{12} \tag{2.1}$$
$$\frac{dB_{pa}}{dt} = f_{12} - f_{23} \tag{2.2}$$
$$\frac{dB_{L}}{dt} = f_{23} - f_{34} \tag{2.3}$$
$$\frac{dB_{pv}}{dt} = f_{34} - f_{45} \tag{2.4}$$
$$\frac{dB_{lv}}{dt} = f_{45} - f_{56} \tag{2.5}$$
$$\frac{dB_{a}}{dt} = f_{56} - f_{67} \tag{2.6}$$
$$\frac{dB_{org}}{dt} = f_{67} - f_{78} \tag{2.7}$$
$$\frac{dB_{v}}{dt} = f_{78} - f_{81} \tag{2.8}$$

Symbol	**Description**	**Units**	**Role**
t	time	min	independent variable
B_i	total blood volume in compartment i	mL	dependent variable
$\bar{V}_i$	blood volume capacity for compartment i	mL	onstant parameter for non-ventricle compartments
P_i	blood pressure in compartment i	$mmHg$	auxiliary variable
C_i	compliance for compartment i	$\frac{mL}{mmHg}$	constant parameter for non-ventricle compartments

Table 2.1: Key model components along with their descriptions.

2.2 Rate Functions

Our choice of rate functions is based, in part, on the following assumptions regarding back-flow of blood and flow of blood through the organs.

Assumptions

1. Back-flow of blood resulting from a negative pressure gradient is impossible.
2. Every flow rate is dependent on a blood pressure gradient.
3. Since valves open and close according to the shift in the blood pressure gradient, heart valves do not explicitly need to be represented by a variable.

Each flow rate function can therefore be equated to the Hagen-Poiseuille Law (Equation (1.2)), where the rate constant $k_{ij} = \frac{1}{R_{ij}}$.

$$f_{12} = \begin{cases} k_{12} * (P_{rv} - P_{pa}) & \text{if } P_{rv} > P_{pa} \\ 0 & \text{if otherwise} \end{cases} \tag{2.9}$$

$$f_{23} = \begin{cases} k_{23} * (P_{pa} - P_L) & \text{if } P_{pa} > P_L \\ 0 & \text{if otherwise} \end{cases} \tag{2.10}$$

$$f_{34} = \begin{cases} k_{34} * (P_L - P_{pv}) & \text{if } P_L > P_{pv} \\ 0 & \text{if otherwise} \end{cases} \tag{2.11}$$

$$f_{45} = \begin{cases} k_{45} * (P_{pv} - P_{lv}) & \text{if } P_{pv} > P_{lv} \\ 0 & \text{if otherwise} \end{cases} \tag{2.12}$$

$$f_{56} = \begin{cases} k_{56} * (P_{lv} - P_a) & \text{if } P_{lv} > P_a \\ 0 & \text{if otherwise} \end{cases} \tag{2.13}$$

$$f_{67} = \begin{cases} k_{67} * (P_a - P_{org}) & \text{if } P_a > P_{org} \\ 0 & \text{if otherwise} \end{cases} \tag{2.14}$$

$$f_{78} = \begin{cases} k_{78} * (P_{org} - P_v) & \text{if } P_{org} > P_v \\ 0 & \text{if otherwise} \end{cases} \tag{2.15}$$

$$f_{81} = \begin{cases} k_{81} * (P_v - P_{rv}) & \text{if } P_v > P_{rv} \\ 0 & \text{if otherwise} \end{cases} \tag{2.16}$$

The piecewise function ensures that there is no back flow if the pressure gradient is less than zero. As an example, blood will not flow in the forward or reverse direction between the right ventricle and pulmonary arteries if $P_{rv} \not> P_{pa}$ (Equation (2.9)).

Although blood flow is driven by pressure gradients, we want to use blood volume as our dependent variable. The expected conservation of total blood volume across all compartments of the model makes it easier to prove the validity of the model. In order to convert between blood pressure and blood volume measures, we also need the rate functions to be in terms of blood volume.

2.3 Pressure/Volume Relationships

The following assumptions are made regarding the pressure/volume relationship for each compartment.

Assumptions

1. Every compartment, except for the ventricles, has constant compliance and volume capacity. Although the pressure/volume relationship can take on a nonlinear form at volumes very far from the unstressed volume, the relationship is fairly linear under normal conditions [14, 29]. Furthermore, it is during times of venoconstriction and venodilation that compliance will shift. This model disregards these mechanisms as short-term responses to regulate blood flow with the assumption that our patient is not experiencing adverse cardiovascular events.

2. Ventricular compliance and volume capacity are highest during diastole and lowest during systole. During diastole, the pressure stays steady as blood is flowing into the relaxed ventricles. This increase in surface area directly corresponds to the increase in volume capacity. During systole, the ventricles contract and shrink, resulting in a significant build-up of pressure.

3. If the total blood volume within a compartment is only made up of unstressed volume ($\bar{V}$), then the corresponding pressure is calibrated to zero. Unstressed volume does not contribute to a change in transmural pressure [2].

Equations (2.17) - (2.24) display the pressures P_i of each compartment in terms of volume capacity $\bar{V}_i$, total blood volume B_i, and compliance C_i. Note that these equations were derived from Equation (1.3). Pressure is written as a function of change in volume ($B_{rv} - \bar{V}_{rv}$) over compliance.

$$P_{rv} = \begin{cases} \frac{B_{rv} - \bar{V}_{rv}(t)}{C_{rv}(t)} & \text{if } B_{rv} > \bar{V}_{rv}(t) \\ 0 & \text{if otherwise} \end{cases} \tag{2.17}$$

$$P_{pa} = \begin{cases} \frac{B_{pa} - \bar{V}_{pa}}{C_{pa}} & \text{if } B_{pa} > \bar{V}_{pa} \\ 0 & \text{if otherwise} \end{cases} \tag{2.18}$$

$$P_{L} = \begin{cases} \frac{B_{L} - \bar{V}_{L}}{C_{L}} & \text{if } B_{L} > \bar{V}_{L} \\ 0 & \text{if otherwise} \end{cases} \tag{2.19}$$

$$P_{pv} = \begin{cases} \frac{B_{pv} - \bar{V}_{pv}}{C_{pv}} & \text{if } B_{pv} > \bar{V}_{pv} \\ 0 & \text{if otherwise} \end{cases} \tag{2.20}$$

$$P_{lv} = \begin{cases} \frac{B_{lv} - \bar{V}_{lv}(t)}{C_{lv}(t)} & \text{if } B_{lv} > \bar{V}_{lv}(t) \\ 0 & \text{if otherwise} \end{cases} \tag{2.21}$$

$$P_{a} = \begin{cases} \frac{B_{a} - \bar{V}_{a}}{C_{a}} & \text{if } B_{a} > \bar{V}_{a} \\ 0 & \text{if otherwise} \end{cases} \tag{2.22}$$

$$P_{org} = \begin{cases} \frac{B_{org} - \bar{V}_{org}}{C_{org}} & \text{if } B_{org} > \bar{V}_{org} \\ 0 & \text{if otherwise} \end{cases} \tag{2.23}$$

$$P_{v} = \begin{cases} \frac{B_{v} - \bar{V}_{v}}{C_{v}} & \text{if } B_{v} > \bar{V}_{v} \\ 0 & \text{if otherwise} \end{cases} \tag{2.24}$$

Modeling nonlinear ventricular compliance or its inversely related counterpart, elastance, is not entirely novel. In one model, a linear piecewise function for elastance was used to match the pulsating shape of ventricular pressure [8]. In our model, sine functions for ventricular compliance and volume capacity are fit to the cardiac cycle and the ventricular blood volume

graph. Using sine functions instead of linear functions as the non-constant pieces of these equations makes certain that it is differentiable at each point in the cardiac cycle.

The parameters of the sine functions are defined (Equations (2.25) - (2.28)). Parameters a, b, and c are characteristics of the timing of the cycle: a represents the time that the systolic period begins, b is the time at which peak pressure is reached during the systolic period, and c is the time that the systolic period ends. f and s are determined by the frequency of the beats and the center of the pressure/volume curves, while m and a are the mean values and the amplitude of the sine curve. mx must be equal to m in order for the constant piece to intersect perfectly with the sine piece at time c. As a result, both m and mx are the maximum volume capacity values. Figure 2.2 shows the simultaneous fluctuations in volume capacity and compliance from our model.

$$\bar{V}_{lv}(t) = \begin{cases} m1 - a1 * \sin(f1 * (T - s1)) & \text{if } a \leq T \leq b \\ m2 - a2 * \sin(f2 * (T - s2)) & \text{if } b < T \leq c \\ mx1 & \text{if otherwise} \end{cases} \tag{2.25}$$

$$\bar{V}_{rv}(t) = \begin{cases} m3 - a3 * \sin(f1 * (T - s1)) & \text{if } a \leq T \leq b \\ m4 - a4 * \sin(f2 * (T - s2)) & \text{if } b < T \leq c \\ mx2 & \text{if otherwise} \end{cases} \tag{2.26}$$

$$C_{lv}(t) = \begin{cases} m5 - a5 * \sin(f1 * (T - s1)) & \text{if } a \leq T \leq b \\ m6 - a6 * \sin(f2 * (T - s2)) & \text{if } b < T \leq c \\ mx3 & \text{if otherwise} \end{cases} \tag{2.27}$$

$$C_{rv}(t) = \begin{cases} m7 - a7 * \sin(f1 * (T - s1)) & \text{if } a \leq T \leq b \\ m8 - a8 * \sin(f2 * (T - s2)) & \text{if } b < T \leq c \\ mx4 & \text{if otherwise} \end{cases} \tag{2.28}$$

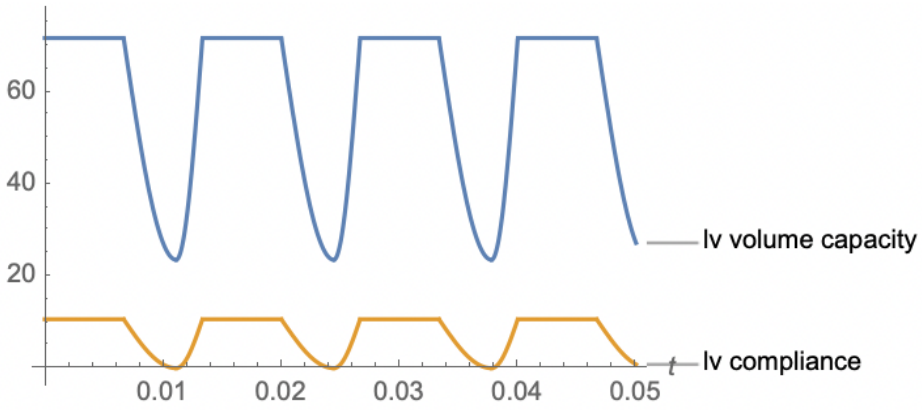

Figure 2.2: Plot of left ventricular unstressed volume and compliance using the above piece-wise functions.

So, our final model consists of differential equations (DE) (2.1) - (2.8), with each f_{ij} given by Equations (2.9) - (2.16) and each P_k given by Equations (2.17) - (2.24). With the complete set of equations defined, the differential equations can be solved.

2.4 Model Analysis

A Mathematica notebook was set up with the model equations and parameter values. Each compartment has a differential equation within the NDSolve[] function that gives a solution for total blood volume B as a function of time t (Equations (2.1) - (2.8)). Initial conditions for blood volume for each compartment and a time range are required as a part of this Initial Value Problem (IVP). Initial conditions are based on average values for total blood volume (Table 2.2).

Blood pressure is also a valuable variable to use when comparing outcomes of the IVP since we can change between blood volume and blood pressure by Equation (2.17) - (2.24). Consequently, blood pressure plots change in response to changing the IVP parameters and solution.

2.5 Choosing the Parameters

In total, there are 41 parameters (excluding the initial conditions). They are made up of compliances and volume capacities, ventricular compliances and volume capacities, and rate constants. Chapter 3 briefly discusses difficulties in confidently selecting a set of parameter values to emulate normal hemodynamic circumstances. There is generally a lack of human hemodynamic data for compliance, volume capacity, and resistance. Many models have relied on animal experimentation and then scale their results by weight, but this translation might be oversimplified.

	Blood Pressure ($mmHg$)	**Total Blood Volume** (mL)	**Volume Capacity** (mL)	**Compliance** $\left(\frac{mL}{mmHg}\right)$	**Resistance** ($\frac{mmHg*min}{mL}$)
Right Ventricle	5-25 [36]	EDV:176 [29]	53.5-103 [29]	1.89-29.15 [29]	0.0002517 [29]
Pulmonary Arteries	8-20 [19]	235 [45]	123 [45]	6.560 [45]	0.00098784 [29]
Lungs	14 [Estimated]	106 [29]	29.4 [29]	9.12 [Estimated]	0.00076419 [29]
Pulmonary Veins	8-12 [Estimated]	297 [45]	120 [45]	25.37 [45]	0.00000995 [29]
Left Ventricle	15-120 [36]	EDV:126 [29]	23.7-71.8 [29]	0.19-10.18 [29]	0.00013479 [29]
Arteries	80-120 [13]	1011 [45]	611 [45]	4 [45]	0.00700427 [29]
Generic Organ	60 [Estimated]	256 [29]	71 [29]	5.77 [Esimated]	0.00825423 [29]
Veins	8-12 [40]	3455 [45]	2900 [45]	111.111 [45]	0.00138447 [29]

Table 2.2: Set of hemodynamic values that play a crucial role in choosing model parameters. Values are from previous reputable mathematical models, animal experiments, or estimated based on what appears to create a good fit.

For arteries and veins, parameter values are calculated from many smaller categories provided by math models (Table 2.2). Resistances are summed, compliances are averaged, and total blood volume and capacity are summed in order to calculate values for the larger compartments in our model. Volumes are summed in order to conserve total blood volume across the system. Since the chain of these blood vessels can be treated as a series circuit, resistances are summed [29]. Note that the rate constant k_{ij} values are calculated as $\frac{1}{R}$ since they are inversely proportional. The generic organ provided the most flexibility in setting parameter values because it is not associated with one specific systemic organ. Theoretically, every organ would have unique parameter values and varying blood flow rates across the capillaries and tissue. This assumption will be considered as we append the organ systems to our model in the future.

Equations (2.29) - (2.49) list the left and right ventricular volume capacity and compliance parameters. We consider a cardiac period of 0.8 seconds, or $\frac{1}{75}$ of a minute.

$$m1 = m2 = 71.8 \tag{2.29}$$
$$a1 = a2 = 48.1 \tag{2.30}$$
$$mx1 = 71.8 \tag{2.31}$$
$$m3 = m4 = 103 \tag{2.32}$$
$$a3 = a4 = 49.5 \tag{2.33}$$
$$mx2 = 103 \tag{2.34}$$
$$m5 = m6 = 10.8 \tag{2.35}$$
$$a5 = a6 = 10.61 \tag{2.36}$$
$$mx3 = 10.8 \tag{2.37}$$
$$m7 = m8 = 29.15 \tag{2.38}$$
$$a7 = a8 = 27.26 \tag{2.39}$$
$$mx4 = 29.15 \tag{2.40}$$
$$f1 = \frac{450\pi}{4} * \frac{2\pi}{4/3 * \text{cardiac period}} \tag{2.41}$$
$$s1 = \frac{3}{450} * 1/2 \text{ of cardiac period} \tag{2.42}$$
$$f2 = \frac{450\pi}{2} * \frac{2\pi}{2/3 * \text{cardiac period}} \tag{2.43}$$
$$s2 = \frac{4}{450} * 2/3 \text{ of cardiac period} \tag{2.44}$$
$$a = \frac{3}{450} * 1/2 \text{ of cardiac period} \tag{2.45}$$
$$b = \frac{4}{450} * 5/6 \text{ of cardiac period} \tag{2.46}$$
$$c = \frac{1}{75} * \text{cardiac period} \tag{2.47}$$
$$T = t - n[t] * c(\text{used to create a repeating cycle}) \tag{2.48}$$
$$n[t] = \left| \left\lceil \frac{t}{c} \right\rceil - 1 \right| \tag{2.49}$$

The literature values in Table 2.2 serve as the basis of our model parameters and provide necessary context as we judge the results of our model tests.

Chapter 3

Simulations and Tests

Our goal is test our model to make sure that the results are consistent with what is already known about normal circulatory system function. The plots from Section 3.2, 3.3, and 3.4 are from running simulations on our model; they ultimately demonstrate that our model results are consistent with the literature and our model appears to uphold the principles of hemodynamics.

3.1 Assumptions

In order to determine parameter values and run purposeful simulations, a hypothetical healthy patient is considered with the following assumptions.

Assumptions

1. The patient is a young and healthy 70 kg male that has normal hemodynamic measures. Aortic pressure should be in the 80-120 mmHg range and stroke volumes should be normal.

2. The patient is not undergoing any hemodynamic stress where they would be losing blood. Although each blood vessel with experience fluctuations in blood volume, the

patient's total blood volume will remain constant.

3.2 Validating Blood Pressure and Valves

Since there is a lot of information regarding normal blood pressure ranges for the ventricles and major blood vessels, we investigate the changing blood pressures for the pulmonary system with the right ventricle and systemic system with the left ventricle.

Every blood vessel downstream of the right ventricle is expected to consistently have a lower blood pressure than its predecessor (Figure 3.1). The same trend occurs for the systemic vessels downstream of the left ventricle (Figure 3.2).

We can further look into the functioning of the valves from these figures. Early on during systole, the right ventricular pressure rises above pulmonary arterial pressure and the pulmonary valve opens. After the ventricle contracts and pressure decreases, pressure falls below the pulmonary arteries and the pulmonary valve will close. The same holds true for the left ventricular pressure and aortic pressure due to the aortic valve. In addition, it is observed that the right ventricular pressure falls within 5 - 30 mmHg and left ventricular pressure ranges from 10-115 mmHg, closely matching the literature. However, the aortic pressure is only 80 - 105 mmHg, resulting in a need for better parameter values to increase the amplitude of the aortic pressure curve.

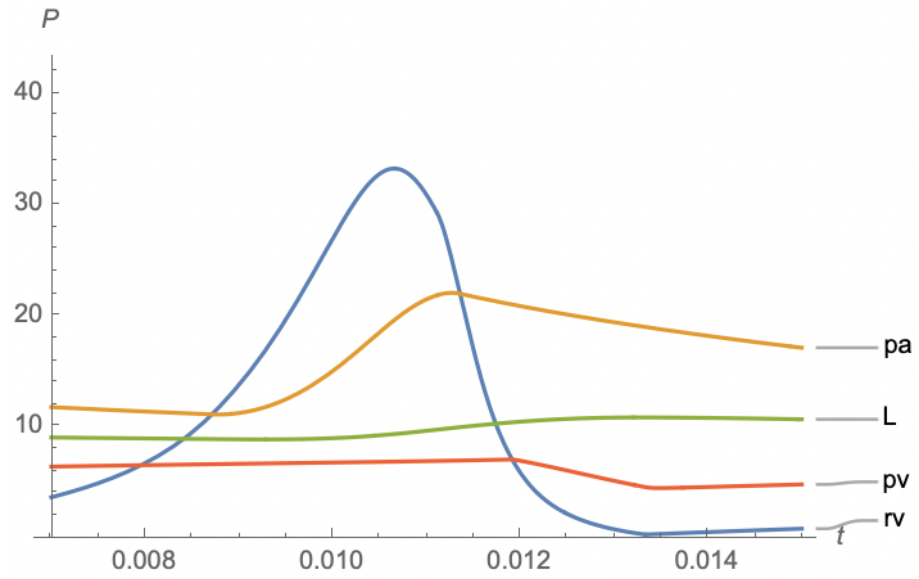

Figure 3.1: Plot of blood pressure for the right ventricles P_{rv}, pulmonary arteries P_{pa}, lungs P_L, and pulmonary veins P_{pv} for a single cardiac cycle.

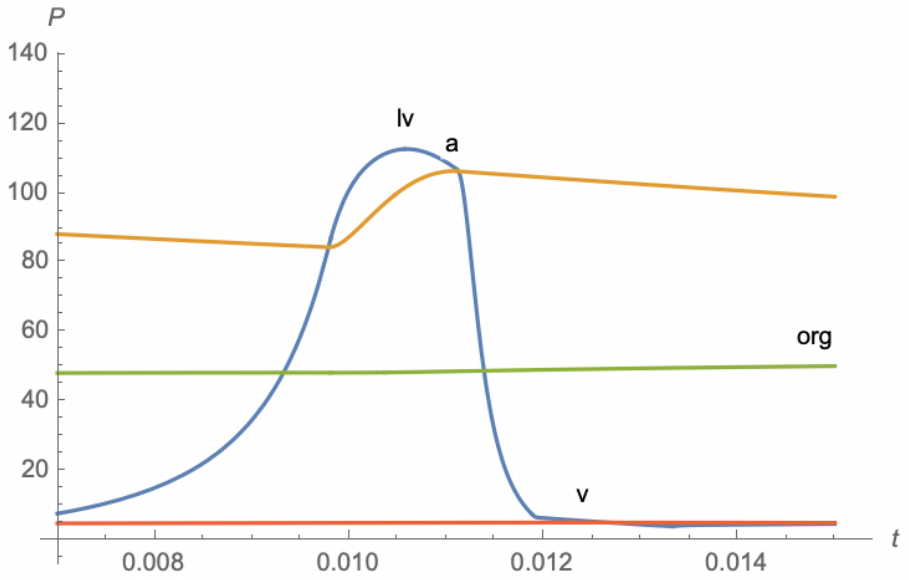

Figure 3.2: Plot of blood pressure for the left ventricles P_{lv}, arteries P_a, generic organ P_{org}, and veins P_v for a single cardiac cycle.

3.3 Validating Total Blood Volume

From the previously stated assumptions, each compartment is expected to display stable solutions for total blood volume and the sum of these blood volumes will remain constant. Figure 3.3 shows that all pulmonary blood vessels and the right ventricle reach equilibrium volume after approximately 0.12 minutes. While all of vessels experience short bursts of changing volumes, the volumes appear to have a steady-state equilibrium.

The left ventricle and systemic system plot shows solutions that are stable from the very beginning (Figure 3.4). Although the the graph appears to show less cyclic changes in volumes across the systemic vessels, the graph is highly skewed by the large volume of the veins. By creating an additional function for the sum of the blood volume in all of the compartments, we can confirm that the amount of blood circulating in the whole system is constant.

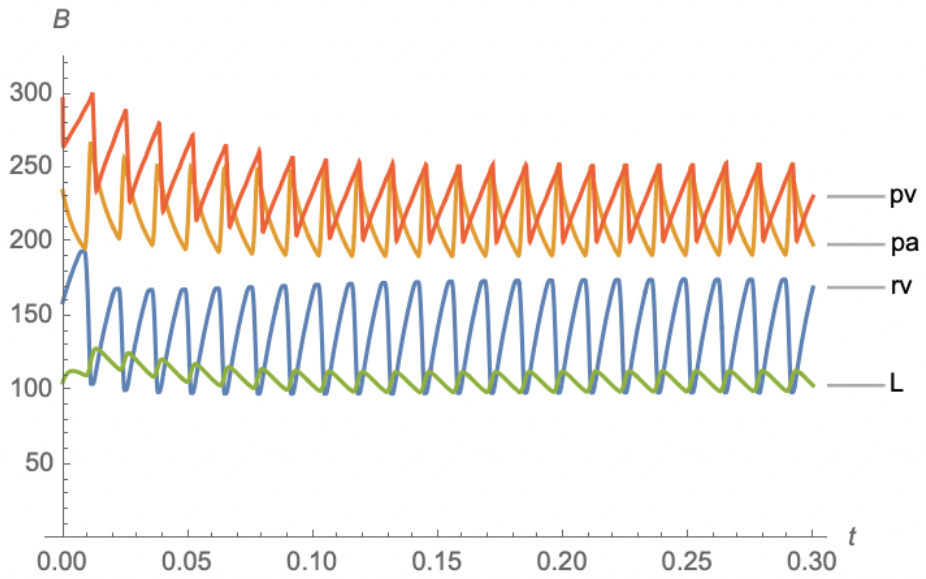

Figure 3.3: Plot of blood volume for the right ventricles B_{rv}, pulmonary arteries B_{pa}, lungs B_L, and pulmonary veins B_{pv}.

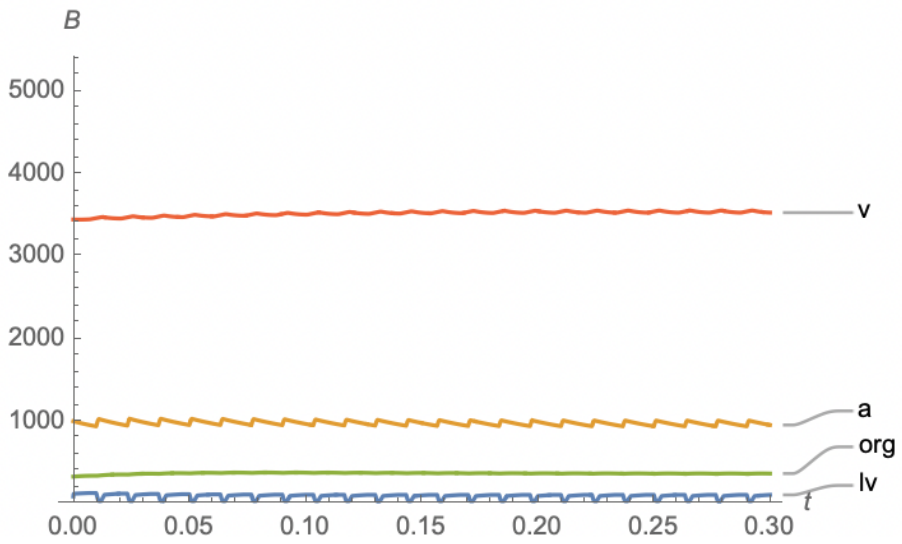

Figure 3.4: Plot of blood volume for the left ventricles B_{lv}, arteries B_a, generic organ B_{org}, and veins B_v.

3.4 Validating Stroke Volume

Now, we determine if the left and right ventricles are ejecting the expected amount of blood each cardiac cycle. Figure 3.5 reveals that the right ventricle has $RVEDV = 170$ and $RVESV = 100$ mL for stable cardiac cycles. Then $RVSV = 70$ mL. While the $RVEDV$ is very close to the value mentioned in Table 2.2, the $RVSV$ is 15 mL lower than another source [34]. Since stroke volume is individualistic, we conclude that 70 mL falls within a wide range of normal values.

Figure 3.6 indicates that the left ventricle has roughly $LVEDV = 120$ and $LVESV = 45$ mL after stabilizing. As a result, $LVSV = 75$ mL. The $LVEDV$ is very close to the value given in Table 2.2, but the values do fall short from another source [34]. Again, we assume that 75 mL falls with a large normal range for left ventricular stroke volume. In addition, the close equality between $LVSV$ and $RVSV$ preserves the Frank-Starling Law from Section 1.3.

In conclusion, both ventricles eject the expected amount of blood into the pulmonary arteries and aorta.

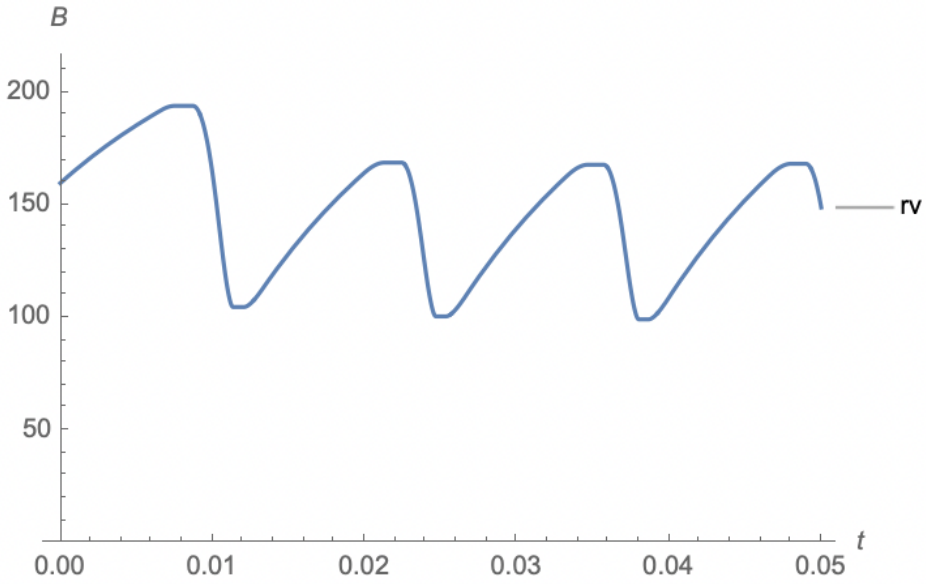

Figure 3.5: Plot of blood volume of the right ventricle B_{rv} for three cardiac cycles.

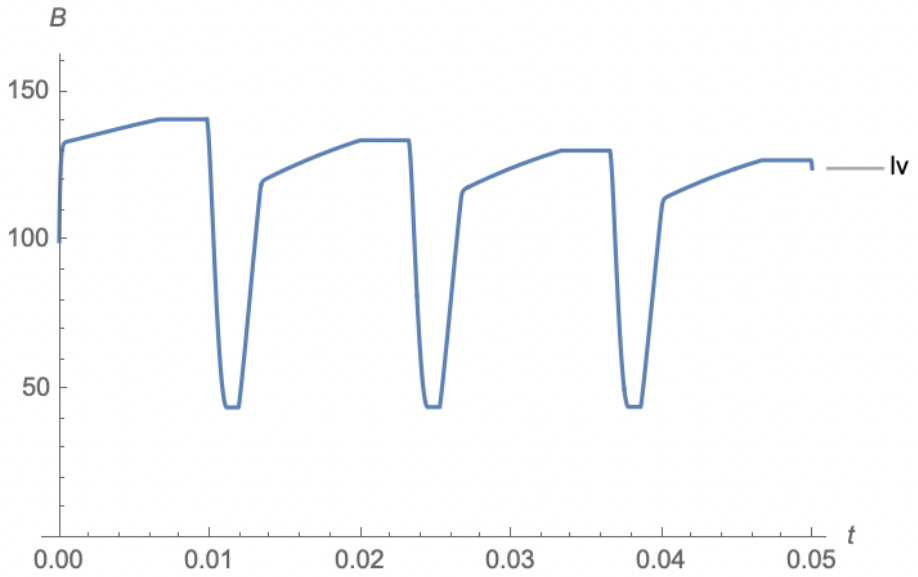

Figure 3.6: Plot of blood volume of the left ventricle B_{lv} for three cardiac cycles.

320 Now that our model has been proven to accurately simulate blood flow in the circulatory

system, we can move forward with assessing our model's ability to transfer oxygen, drugs, and other vital substances.

Chapter 4

Two Extensions: Oxygen and Hypertension

These two extensions describe how our current model could be modified to include the transfer of oxygen and the delivery of drugs. Future directions for these applications are explained in the context of our subsequent goal to create a major organ systems model.

4.1 Oxygen Delivery and Consumption

Oxygen is an essential reactant for various functions on the cellular level, including aerobic cellular respiration. Oxygen molecules are bound to haemoglobin found in erythrocytes (red blood cells), which are distributed across the body following uptake [5]. Oxygen concentrations can change based on the binding affinity to haemoglobin and successful uptake of oxygen by the alveoli, so blood flow alone does not dictate oxygen delivery rates. Equation (4.1) gives oxygen delivery D_{O_2} in terms of flow rate Q and concentration of arterial oxygen C_{aO_2} [35].

$$D_{O_2} = Q * C_{aO_2} \tag{4.1}$$

Concentration of arterial oxygen C_{aO_2} is dependent on concentration of hemoglobin, saturation of arterial oxygen, and partial pressure of arterial oxygen. Oxygen consumption relies on the difference in oxygen content in the arteries and veins connected to the organ. Thus, venous oxygen concentration (C_{vO_2}) is an additional parameter necessary to calculate the concentration gradient across the organ. Equations (4.2) - (4.6) show how V_{O_2} can be written as a proportion of D_{O_2} through substitution [6].

$$V_{O_2} = Q * (C_{aO_2} - C_{vO_2}) \tag{4.2}$$
$$V_{O_2} = D_{O_2} - (Q * C_{vO_2}) \tag{4.3}$$
$$V_{O_2} = D_{O_2} - \frac{D_{O_2} * C_{vO_2}}{C_{aO_2}} \tag{4.4}$$
$$V_{O_2} = D_{O_2} * (1 - \frac{C_{vO_2}}{C_{aO_2}}) \tag{4.5}$$
$$V_{O_2} = D_{O_2} * \frac{C_{aO_2} - C_{vO_2}}{C_{aO_2}} \tag{4.6}$$

$\frac{C_{aO_2} - C_{vO_2}}{C_{aO_2}}$ can be referenced as the extraction ratio E, the fraction of blood that is taken up by the tissue (Equation (4.7)).

$$V_{O_2} = D_{O_2} * E \tag{4.7}$$

Every organ has unique values for regional flow rate, oxygen delivery rate, extraction ratio, and consumption. These major differences stem from the unique arteries (i.e. renal artery for the kidneys and the hepatic artery for the liver) that are connected to the organs. The difference in circuitry of the organ systems allows for local regulation of blood flow. An increase in extraction ratio could allow for an organ to maintain constant oxygen consumption during periods of below-normal delivery rates. In fact, this mechanism happens during

intense exercise [37]. The heart, skeletal muscle, and brain have the highest extraction ratios. The brain can only survive for 3 minutes without an adequate amount of oxygen available [26].

The critical D_{O_2} represents the oxygen delivery rate for which lower rates have a linear relationship with oxygen consumption [6]. For values above D_{O_2}, the extraction ratio or blood flow is adjusted to maintain a constant consumption rate. The heart is the only major organ known to display a completely dependent relationship between oxygen consumption and delivery [37]. While the exact pathology of blood flow regulation is unknown, vasodilation and vasoconstriction are believed to alter the surface area of the arteries and thus adjust blood flow rates. However, we are limited by our uncertainty in how the body distributes oxygen among the vital organs in very extreme hypoxic events [37].

Once our model can successfully simulate oxygen transport dynamics, we can use the same modeling mechanisms to simulate the transport other important substances (e.g. nutrients, waste products, medications) throughout the body. These mechanisms will crucial for modeling sequential organ failure and sepsis.

4.2 Evaluation of Hypertension Medications

Hypertension is a condition of elevated blood pressure and antihypertensive medications are commonly prescribed to treat chronic and acute hypertension [3]. The drugs are classified according to their target receptor. Diuretics, renin-angiotensin system inhibitors, calcium channel blockers, and beta-blockers are the most common classes of antihypertensives [49].

In broad terms, diuretics work to inhibit sodium, chloride, and/or potassium absorption or reabsorption [30]. As a result, blood volume and cardiac output decrease [49]. Beta blockers (BB) block the beta-1 adrenergic receptors, which is activated by the neurotransmitter norepinephrine. Since norepinephrine is critical for stimulating the heart, the blockage re-

sults in decreased heart rate, contraction, and ultimately lower cardiac output and blood pressure [30].

Calcium channel blockers (CBB) block the entry of of calcium ions into the smooth blood vessel walls. The net-effect is a decline in force of contraction of these blood vessels, known as vasodilation [30]. Calcium channel blockers can either act on only the arteries or arteries and cardiac muscles. The renin-angiotensin system (RAS) is composed of multiple pathways and provides the opportunity for different target inhibitors. There are ACE inhibitors, angiontension rececptor blockers, and renin inhibitors [30]. Since angiontensin II leads to increased sodium and water retention and vasoconstriction, inhibitory mechanisms will limit these responses and decrease blood pressure [30].

Most of these drugs are only available for oral administration, but clonidine, a centrally acting agonist, became the first antihypertensive drug available as a patch [39]. Transdermal delivery has some clear advantages; lack of first-pass metabolism and decreased dose frequency improve patient compliance and limit gastrointestinal (GI) side effects [24]. The oral and patch versions of clonidine have been shown to display similar efficacy, but the patch is associated with more side effects (dry mouth, drowsiness, etc.) [39].

Other than the characterization of hypertension in a patient and the properties of the available drugs, genetics and preexisting conditions influence drug response and any adverse reactions. For example, a kidney disease patient will be recommended to take an ACE inhibitor and an angiotensin receptor blocker while patients experiencing heart failure or heart attacks will be told to avoid CCBs [30]. If a patient is not responding to a single class, combination therapy is usually administered, with CCBs, BBs, and alpha blockers being the most common combination [21].

In addition to their unique mechanisms of action (MOA), antihypertensive drugs possess different pharmacokinetic and pharmacodynamic parameters.

4.3 Modeling Pharmacokinetics

Pharmacokinetics is the science of the absorption, distribution, metabolism, and excretion of a drug in the body [4]. Some models include the GI system as a compartment [1], while other models elect to focus on distribution of the drug to the different organs [4]. First-pass metabolism, which is drug metabolism that occurs (due to interactions in the stomach and liver) prior to entering the systemic circulation, is a major disadvantage of drugs taken orally [4]. First-pass metabolism greatly influences the bioavailability, which is the proportion of drug that enters the bloodstream. For transdermal drugs, proportion of drug that successfully passes through the dermis and epidermis layers is dependent on the lipid solubility property of the drug [4].

Figure 4.1 shows a compartment diagram for pharmacokinetics of a drug taken orally. This compartment diagram does not apply to other delivery systems, such as transdermal patches, because it includes the GI system as the uptake location prior to entering the bloodstream. We were inspired by [1] to include the GI system as a compartment in order to best demonstrate differences between drugs given their unique bioavailability properties. Many other models [1], [4] do not include a rate of administration g_{01}, but in our case, we need it to schedule the administration of multiple doses.

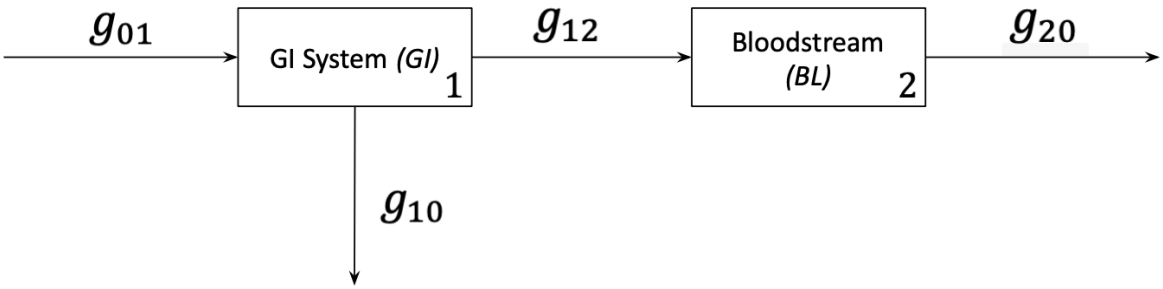

Figure 4.1: Compartment diagram for pharmacokinetics of oral delivery of drugs. g_{01} is the administration rate, g_{10} is the rate of which the drug is metabolized by the GI system and turned inactive, g_{12} is the rate of absorption into the bloodstream, and g_{20} is the rate of elimination. The kidneys usually excrete water-soluble drug metabolites.

Again, we set up our differential equations for each compartment given the flow rates in and out (Equation (4.8) - (4.9)). Amount of drug A is the dependent variable measured for the GI compartment and concentration of the drug C is the dependent variable for BL compartment. Volume of distribution VD is used to convert amount (mg) to concentration (mg/mL) (Equation (4.9)). It represents the volume of a fluid that a drug would need to be dissolved in to have the same plasma concentration [4]. VD is a characteristic of a drug that can be often be found on the FDA or drug manufacturer's website.

$$\frac{dA_{GI}}{dt} = g_{01} - g_{12} - g_{10} \tag{4.8}$$

$$\frac{dC_{BL}}{dt} = \frac{g_{12}}{VD} - g_{20} \tag{4.9}$$

In Equation (4.10), d is the dose amount (mg) and d_t is the time it takes for the drug to dissolve in the stomach and become available for absorption into the bloodstream. Equation (4.11) takes the single dose rate $A(t)$ and schedules multiple doses based on the frequency of the dose d_f. The GI will metabolize the $(1 - f)$ proportion of drug prior to it entering the bloodstream, where f is the bioavailability fraction.

$$A(t) = \begin{cases} \frac{d}{d_t} & 0 \leq t \leq d_t \\ 0 & \text{if otherwise} \end{cases} \tag{4.10}$$

$$g_{01} = \sum_{j=1}^{d_n} A(t)(t - (j-1) * d_f) \tag{4.11}$$

$$g_{10} = (1 - f) * k10 * A_{GI} \tag{4.12}$$

$$g_{12} = k12 * f * A_{GI} \tag{4.13}$$

$$g_{20} = k20 * C_{BL} \tag{4.14}$$

Table 4.1 lists common pharmacokinetic parameters of a drug that are traditionally discovered during pre-clinical and clinical trials. Half-life is the amount of time for plasma concentration to decrease by 50%, t_{max} is the time it takes for maximum plasma concentration to be reached, C_{max} is the maximum plasma concentration, and steady-state concentration is the equilibrium concentration reached after multiple doses.

	Clonidine tablets (Catapres)	**Clonidine patch (Catapres)**
Dose (mg)	0.1 (twice a day) [38]	5 (weekly) [44]
Volume of Distribution (mL)	197000 [44]	197000 [44]
Half-life (hrs)	12-16 [43]	12-16 [44]
t_{max} (hrs)	1-3 [43]	within 3 days [33]
C_{max} (ng/mL)	0.2-2 [43]	N/A
Bioavailability (%)	70 [43]	60 [44]
Steady-state Concentration (ng/mL)	0.30-0.35 [23]	0.8 [33]

Table 4.1: Pharmacokinetic parameters for comparison of oral and transdermal delivery systems of clonidine provided by the brand Catapres.

Each compartment has a differential equation within the NDSolve[] function that solves for either amount of drug or drug concentration. Plasma concentration curves are graphed separately for oral and transdermal clonidine drugs.

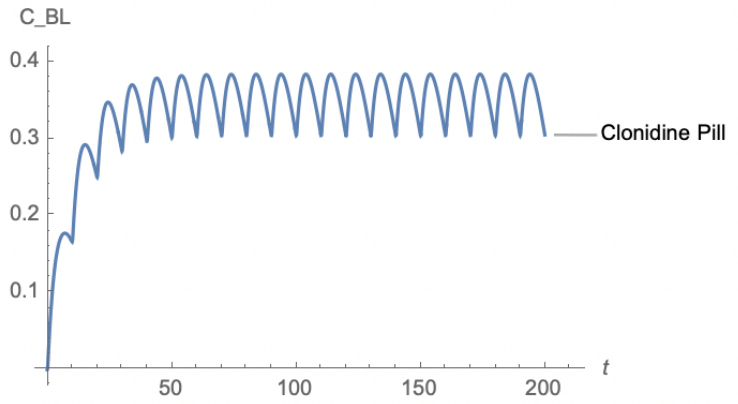

Figure 4.2: Plot of plasma concentration curve (ng/mL) over time (hours) for a 0.1 mg pill of Catapres given every 10 hours.

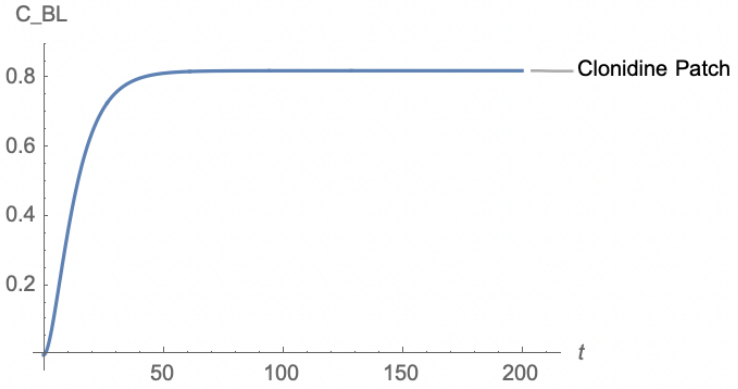

Figure 4.3: Plot of plasma concentration curve (ng/mL) over time (hours) for a 5 mg patch of Catapres replaced every week.

While the clonidine patch does not undergo first-pass metabolism, a bioavailability less than 100% indicates that some portion of the drug is lost before absorption. This is most likely due to the lipid solubility characteristic of the drug and inability for the drug to penetrate the skin and move across the dermis and epidermis layers. We determine that the skin can act as the GI compartment presented in Figure 4.1 for transdermal drugs.

Figure 4.3 shows a higher maximum plasma concentration and steady-state concentration for the clonidine patch than the clonidine pill in Figure 4.2. Since the pill is also more frequently administered than the patch, a patient will experience more acute fluctua-

tions in plasma concentration and potentially varying pharmacological effects. Both plasma concentration curves show equilibrium concentrations that meet the expected steady-state concentrations (Table 4.1).

4.4 Modeling Pharmacodynamics

Pharmacodynamics is the study of how a drug interacts with its target receptor to create pharmacological effects [4]. For hypertension, the expected response would be a significant decrease in blood pressure. Dose-response curves measure the effect of a drug given the dose. Since we do not want to compare dosages, but rather the long-term effects of each drug, it would be necessary to have a concentration-response curve for each drug of interest. We would want to evaluate the decrease in blood pressure given the plasma concentration of the drug in the body. With this information, we can determine the percent change in parameter values that are directly affected by a drug given its MOA. In our model, relevant parameter values are compliance, resistance, and frequency of heart beats (given by the ventricular sine functions).

Chapter 5

Conclusions

While our circulatory system model would benefit from more precise parameter values, the simulations in Chapter 3 display several parallels with known physiology. Our model successfully uses the ventricles to pump blood across the blood vessels, lungs, and an organ for multiple cardiac cycles. We can hypothesize that this model will be able to pump blood to multiple organs that are connected in a parallel circuit. A new compartment would be added for the addition of each major organ system, and new rate functions that connect the organs to their local arteries and veins would be necessary. As mentioned in Chapter 4, these regional flow rates dictate delivery of oxygen and it is crucial for each organ's ability to regulate regional blood flow.

We conclude that this model can serve as the framework of a multiple organ system model to simulate septic infections and sequential organ failure. It could also be worthwhile to further explore the effect of antihypertensive medications with more organ systems represented. Since the GI system metabolizes drugs and the renal system excretes most water-soluble drugs and plays a crucial role in the pathology of hypertension [15], the liver and kidneys would be important additions for drug delivery models. The oral and transdermal pharmacokinetics model could be valuable later on as we integrate treatment options

for cardiovascular conditions and organ damage.

In conclusion, our proposed circulatory system model shows great promise as a foundation for a major organ systems model to examine the net effects of organ dysfunction.

Bibliography

[1] T. Ahmed. Pharmacokinetics of drugs following iv bolus, iv infusion, and oral administration. https://www.intechopen.com/books/basic-pharmacokinetic-concepts-and-some-clinical-applications/pharmacokinetics-of-drugs-following-iv-bolus-iv-infusion-and-oral-administration. Accessed April 10, 2021.

[2] A. Albanese, L. Cheng L, M. Ursino, and N.W. Chbat. An integrated mathematical model of the human cardiopulmonary system: model development. *Am J Physiol Heart Circ Physiol*, 310(7):H899–H921, 2016.

[3] American Heart Association. Types of blood pressure medications. https://www.heart.org/en/health-topics/high-blood-pressure/changes-you-can-make-to-manage-high-blood-pressure/types-of-blood-pressure-medications. Accessed April 10, 2021.

[4] G.M. Brenner and C. W. Stevens. *Pharmacology Fifth Edition*. Elsevier, Philadelphia, 2018.

[5] A. Carreau, B. El Hafny-Rahbi, A. Matejuk, C. Grillon, and C. Kieda. Why is the partial oxygen pressure of human tissues a crucial parameter? small molecules and hypoxia. *J Cell Mol Med*, 15(6):1239–1253, 2011.

[6] R.G. Carroll. *Elsevier's Integrated Physiology*, chapter 7 - The Heart. Mosby, 2007.

[7] J.G. Chaui-Berlinck and L.H.A. Monteiro. Frank-starling mechanism and short-term adjustment of cardiac flow. *J Exp Biol*, 220(pt 23):4391–4398, 2017.

[8] JJ. S. Chen, T. Heldt, G.C. Verghese, and R.G. Mark. Analytical solution to a simplified circulatory model using piecewise linear elastance function. *Computers in Cardiology*, 30:45–48, 2003.

[9] M. Darmon, F. Schortgen, R. Leon, S. Moutereau, J. Mayaux, F. DiMarco, J. Devaquet, C.B. Buisson, and L. Brochard. Impact of mild hypoxemia on renal function and renal resistive index during mechanical ventilation. *Intensive Care Med.*, 35:1031–1038, 2009.

[10] S. Faubel. Pulmonary complications after acute kidney injury. *Adv Chronic Kidney Dis*, 15(3):284–296, 2008.

[11] Centers for Disease Control. What is sepsis? https://www.cdc.gov/sepsis/what-is-sepsis.html. Accessed April 10, 2021.

[12] D.L. Franklin, R.L. Van Citters, and R.F. Rushmer. Balance between right and left ventricular output. *Circulation Research*, 10:17–26, 1962.

[13] E.M. Frese, A. Fick, and H.S. Sadowsky. Blood pressure measurement guidelines for physical therapists. *Cardiopulm Phys Ther J*, 22(2):5–12, 2011.

[14] C.V. Greenway and W.W. Lautt. Blood volume, the venous system, preload, and cardiac output. *Can J Physiol Pharmacol*, 64(4):383–387, 1986.

[15] A. C. Guyton, J. P. Montani, J. E. Hall, and R. D. Jr Manning. Computer models for designing hypertension experiments and studying concepts. *Am J Med Sci*, 295(4):320–326, 1988.

[16] A.C Guyton and T.G. Coleman. *Physical Bases of Circulatory Transport*, chapter Long-term regulation of the circulation: Interrelationships with body fluid volumes. WB Saunders Co, 1967.

[17] V.H. Haase. Mechanism of hypoxia responses in renal tissue. *Journal of the American Society of Nephrology*, 74:537–541, 2013.

[18] R. Hainsworth. The importance of vascular capacitance in cardiovascular control. *News Physiol Sci*, 5(1):250–254, 1990.

[19] G.A. Heresi, O.A. Minai, A. R. Tonelli, J.P. Hammel, S. Farha, J.G. Parambil, and R.A. Dweik. Clinical characterization and survival of patients with borderline elevation in pulmonary artery pressure. *Pulm Circ*, 3(4):916–925, 2013.

[20] I.S. Ho. Visualizing the cardiac cycle: A useful tool to promote student understanding. *J Microbiol Biol Educ.*, 12(1):56–58, 2011.

[21] N. Jarari, N. Rao, J.R. Peela, K.A. Ellafi, S. Shakila, A. R. Said, N. K Nelapalli, Y. Min, K.D. Tun, S. I. Jamallulail, A. K. Rawal, R. Ramanujam, R. N. Yedla, D. K. Kandregula, A. Argi, and L. T. Peela. A review on prescribing patterns of antihypertensive drugs. *Clin Hypertens*, 22(7), 2015.

[22] A.E. Jones, S. Trzeciak, and J.A. Kline. The sequential organ failure assessment score for predicting outcome in patients with severe sepsis and evidence of hypoperfusion at the time of emergency department presentation. *Critical Care Medicine*, 37:1649–1654, 2009.

[23] A. Keränen, S. Nykänen, and J. Taskinen. Pharmacokinetics and side-effects of clonidine. *Eur J Clin Pharmacol*, 13(2):97–101, 1978.

[24] K. Khatoon, M.D. Rizwanullah, S. Amin, S. R. Mir, and S. Akhter. Cilnidipine loaded transfersomes for transdermal application: Formulation optimization, in-vitro and in-vivo study. *Journal of Drug Delivery Science and Technology*, 54, 2019.

[25] C.L Klein, T.S. Hoke, W.F. Fang, C.J. Altmann, I.S. Douglas, and S. Faubel. Interleukin-6 mediates lung injury following ischemic acute kidney injury or bilateral nephrectomy. *Kidney Int*, 74(7):901–909, 2008.

[26] R.M. Leach and D.F. Treacher. Oxygen transport — 2. tissue hypoxia. *BMJ*, 317(7169):1370–1373, 1998.

[27] J.R. Levick. *An Introduction to Cardiovascular Physiology 4th Edition*. CRC Press, London, 2003.

[28] T.Y. Lin, Y.G. Chen, C.L. Lin, and C.H. Kao. Increased risk of acute kidney injury following pneumococcal pneumonia: A nationwide cohort study. *PLoS One*, 11(6):e0158501, 2016.

[29] M.L. Neal and J.B. Bassingthwaighte. Subject-specific model estimation of cardiac output and blood volume during hemorrhage. *Cardiovasc Eng (Dordrecht, Netherlands)*, 7(3):97–120, 2007.

[30] Q. Nguyen, J. Dominguez, L. Nguyen, and N. Gullapalli. Hypertension management: an update. *Am Health Drug Benefits*, 3(1):47–56, 2010.

[31] S.A. Novosad, M.R. Sapiano, C. Grigg, J. Lake, M. Robyn, G. Dumyati, C. Felsen C, D. Blog, E. Dufort, S. Zansky, K. Wiedeman, L. Avery, R.B. Dantes, J.A. Jernigan JA, S.S. Magill SS, A. Fiore, and L. Epstein. Vital signs: Epidemiology of sepsis: Prevalence of health care factors and opportunities for prevention. *MMWR Morb Mortal Wkly Rep*, 65(33):864–869, 2016.

[32] A. Oue, Y. Iimura, K. Maeda, and T. Yoshizaki. Association between vegetable consumption and calf venous compliance in healthy young adults. *J Physiol Anthropol*, 39(1):18, 2020.

[33] PDR. clonidine - drug summary. https://www.pdr.net/drug-summary/Catapres-TTS-clonidine-2349. Accessed April 10, 2021.

[34] S.E. Petersen, N. Aung, M.M Sanghvi, F. Zemrak, K. Fung, J.M. Paiva, J.M. Francis, M.Y. Khanji, E. Lukaschuk, A.M. Lee, V. Carapella, Y.J. Kim YJ, P. Leeson, S.K. Piechnik, and S. Neubauer. Reference ranges for cardiac structure and function using cardiovascular magnetic resonance (cmr) in caucasians from the uk biobank population cohort. *J Cardiovasc Magn Reson*, 19(1):18, 2017.

[35] M.R. Pinsky, L. Brochard, and J. Mancebo. *Applied Physiology in Intensive Care Medicine*. Springer-Verlag, Berlin Heidelberg NewYork, 2006.

[36] J. D. Pollock and A. N. Makaryus. *Physiology, Cardiac Cycle*. StatPearls Publishing, Treasure Island (FL), 2020.

[37] J. Roca, R. Rodriguez-Roisin, and P.D. Wagner. *Pulmonary and Peripheral Gas Exchange in Health and Disease*. CRC Press, New York, 2000.

[38] RxList. Catapres (clonidine) tablets for hypertension (high blood pressure): Symptoms, uses, dosage, side effects, interactions, warnings. https://www.rxlist.com/catapres-drug.htm. Accessed April 10, 2021.

[39] R. Selvam, A. Singh, and T. Sivakumar. Transdermal drug delivery systems for antihypertensive drugs - a review. *Int J Pharm Biomed Res*, 1(1):1–8, 2010.

[40] P. Shah and M.A. Louis. *Physiology, Central Venous Pressure*. StatPearls Publishing, Treasure Island (FL), 2020.

[41] R.A. Sharkey, E.M.T. Mulloy, and S.J O'Neil. Acute effects of hypoxaemia, hyperoxaemia, and hypercapnia on renal blood flow in normal and renal transplant subjects. *European Respiratory Journal*, 12:653–657, 1998.

[42] S. Sutera and R. Skalak. The history of poiseuille's law. *Annu. Rev. Fluid Mech*, 25:1–19, 1993.

[43] Boehringer Ingelheim International GmbH. Catapres (clonidine hydrochloride, usp). https://www.accessdata.fda.gov/drugsatfda_docs/label/2012/017407s037lbl.pdf. Accessed April 10, 2021.

[44] Boehringer Ingelheim International GmbH. Catapres - tts (clonidine). https://www.accessdata.fda.gov/drugsatfda_docs/label/2012/018891s028lbl.pdf. Accessed April 10, 2021.

[45] M. Ursino, M. Antonucci, and E. Belardinelli. Role of active changes in venous capacity by the carotid baroreflex: Analysis with a mathematical model. *Am J Physiol*, 267(6 Pt 2):H2531–H2546, 1995.

[46] M. Ursino and E. Magosso. Acute cardiovascular response to isocapnic hypoxia. i. a mathematical model. *Am J Physiol Heart Circ Physiol*, 279(1):H149–H165, 2000.

[47] L. Zhong, D.N. Ghista, E.Y. Ng, and S.T. Lim. Passive and active ventricular elastances of the left ventricle. *Biomed Eng Online*, 4:10–, 2005.

[48] HG. Zimmer. Who discovered the frank-starling mechanism? *News Physiol Sci*, 17(5):181–184, 2002.

[49] A. Zisaki, L. Miskovic, and V. Hatzimanikatis. Antihypertensive drugs metabolism: an update to pharmacokinetic profiles and computational approaches. *Curr Pharm Des*, 21(6):806–822, 2015.